PHYSICAL REVIEW D **95,** 075021 (2017)

Collider phenomenology of $e^-e^- \to W^-W^-$

Kai Wang, Tao Xu, and Liangliang Zhang
Zhejiang Institute of Modern Physics and Department of Physics, Zhejiang University, Hangzhou, Zhejiang 310027, China
(Received 14 October 2016; published 14 April 2017)

The Majorana nature of neutrinos is one of the most fundamental questions in particle physics. It is directly related to the violation of accidental lepton number symmetry. This motivated enormous efforts into the search of such processes; among them, one conventional experiment is the neutrinoless double-beta decay ($0\nu\beta\beta$). On the other hand, there have been proposals of future electron-positron colliders as a "Higgs factory" for the precise measurement of Higgs boson properties, and it has been proposed to convert such a machine into an electron-electron collider. This option enables a new way to probe TeV Majorana neutrinos via the inverse $0\nu\beta\beta$ decay process ($e^-e^- \to W^-W^-$) as an alternative and complementary test to the conventional $0\nu\beta\beta$ decay experiments. In this paper, we investigate the collider search for $e^-e^- \to W^-W^-$ in different decay channels at future electron colliders. We find that the pure hadronic channel, the semileptonic channel with a muon, and the pure leptonic channel with a dimuon have the most discovery potential.

DOI: 10.1103/PhysRevD.95.075021

I. INTRODUCTION

Enormous neutrino oscillation experiments in the last two decades have provided definite evidence for nonzero neutrino masses and the mixing between different flavors [1–3]. Even though the recent discovery of a Higgs-like boson has significantly improved our knowledge of the generation of the standard model (SM) fermion masses, being tiny but electric neutral, the origin of the neutrino mass remains an open question. First of all, if neutrino masses arise from Yukawa couplings as the same mechanism as quarks and charged leptons, one immediately encounters the $\mathcal{O}(10^{-12})$ hierarchy in y_ν/y_t. A second argument arises from the prediction of electric charge quantization. Anomaly-free conditions determine $U(1)_Y$ as the unique $U(1)$ gauge symmetry in the SM up to a normalization factor [4]. Though extending the SM with a millicharged Dirac neutrino does not explicitly violate the anomaly-free conditions, the hypercharge assignment is no longer uniquely determined unless the neutrino is a Majorana particle [5]. On the other hand, the bound on the neutrino electric charge Q_ν is $|Q_\nu| \lesssim (0.5 \pm 2.9) \times 10^{-21} e$ (68% C.L.) by assuming charge conservation in β decay, $n \to p + e^- + \bar{\nu}_e$ [6,7], and $|Q_\nu| < 2 \times 10^{-15} e$ from SN1987A astrophysics observation [8]. These facts motivate the study of Majorana neutrinos.

Taking the effective theory approach, the Majorana mass term is from the nonrenormalizable Weinberg operator $(y_{ij}/\Lambda_L)\ell_i\ell_j\Phi\Phi$ [9] with dimensionless coupling y_{ij}. This dimension-five operator breaks lepton number by two units ($\Delta L = 2$) and indicates new physics at some specific Λ_L scale. One elegant observation is that $\mathcal{O}(\mathrm{eV})$ neutrino mass can be a consequence of M_{GUT} suppression. The simplest realization is the so-called type-I "seesaw" mechanism, where a SM singlet neutrino N forms the Dirac mass term $y_\nu \bar{\ell}_L N \Phi$ with a leptonic $SU(2)_L$ doublet and a Majorana mass term $M_R \overline{N^c} N$ by itself [10–13]. The SM singlet N can be accommodated in the spinor representation of the $SO(10)$ GUT representation as $16 = 10 + \bar{5} + 1$. The lighter mass eigenstates are then identified as light neutrinos, and the heavy ones with mass $M_N \sim M_{\mathrm{GUT}}$ can only be searched for through indirect effects.

Further access to low seesaw scales exists in extended models where the higher-dimensional Weinberg operator $[\mu_{ij}^{(n-1)}/\Lambda_L^n]\ell_i\ell_j\Phi\Phi$ allows more freedom in choosing the Λ_L scale and the μ coefficient for neutrino mass generation. The low-scale seesaw extension, on the other hand, calls for heavy-neutrino ν_N searches at various scales. At present, there are several types of such experiments but not a specific one to cover all regions. Among them, the $0\nu\beta\beta$ decay experiment is the most important one to discover the lepton number violating (LNV) process with $\Delta L = 2$. There has been no signal event observed by GERDA and KamLAND-Zen Collaborations so far [14,15]. This provides the strongest bounds on the neutrino mixing $|V_{eN}|^2$ below $10^{-8} \sim 10^{-6}$ in a wide M_N window from 1 MeV to 500 GeV. However, this bound is significantly weakened when there are more than two Majorana neutrino flavors because Majorana CP phases introduce cancellation between $0\nu\beta\beta$ decay amplitudes [16,17]. In addition, there are direct and indirect constraints when M_N varies from eV to TeV [18–35]. Experiments with abundant mesons could probe light ν_N in meson decay $X^\pm \to \ell^\pm \nu_N$. The branching ratio is proportional to $|V_{\ell N}|^2$, and the lepton spectrum deviates from the usual active neutrino case. Further detection of decays with same-sign dileptons could be evidence of the Majorana property. In LHCb and Belle experiments where precise B-meson measurement is available, LNV decay constraints on $|V_{\ell N}|^2$ are around $\mathcal{O}(10^{-4})$ with M_N close to m_B [18,19]. For regions below m_D, the

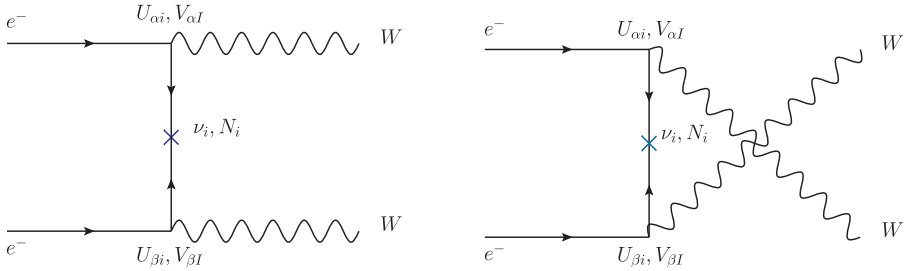

(a) t-channel (b) u-channel

FIG. 1. Inverse $0\nu\beta\beta$ decay.

dubbed beam dump search could detect decay products of those ν_N from D mesons. The Charm and NuTeV experiments could, respectively, push $|V_{eN}|^2$ and $|V_{\mu N}|^2$ to below 10^{-6}, while the PS191 and E949 bounds below 450 MeV are even stronger [20–24]. The most severe bound in this region is close to 10^{-9} when M_N is around 300 MeV. For even smaller M_N, the E_ℓ peak strategy could be used, for example, in $\pi \to eN$ [30] and $K \to \mu N$ [31] processes. When ν_N are heavier than mesons, the Delphi experiment at LEP measured a $Z \to \nu_N \nu$ branching ratio for M_N between 3.5 and 50 GeV, and the corresponding $|V_{\ell N}|^2$ bound is at $\mathcal{O}(10^{-5})$ [32]. As for hadron collider searches, the smoking-gun signature is the same-sign dilepton plus jets without $\not{E}_T$. Both the ATLAS [33] and CMS [34,35] Collaborations have published results with 8 TeV data for M_N up to 500 GeV. However, they are still weaker than the electroweak precision observable (EWPO) bound by constraining the nonunitarity of the leptonic mixing matrix [36],

$$\sum_i |V_{ei}|^2 \leq 2.1 \times 10^{-3}. \tag{1}$$

More detailed analyses are available in [37–39].

As an alternative, the $e^-e^- \to W^-W^-$ scattering process in Fig. 1 mediated by Majorana neutrino exchange is sensitive to the TeV-seesaw scenario. The intriguing feature of this process is that it could be regarded as the inverse of $0\nu\beta\beta$ decay with LNV but that it could occur at colliders. In addition, the destructive interference effects due to the Majorana CP phase in $0\nu\beta\beta$ decay experiments may behave differently as a result of energy scale dependence. According to [40], the unitarity of this process is automatically preserved with the seesaw relation of left-handed electron-neutrino Majorana mass. In some extended models with a Higgs triplet, this process could also be mediated by a doubly charged Higgs boson in the s channel. This case has been studied in [41–44]. Previous work on the $e^-e^- \to W^-W^-$ search can be found in [40–51].

Recently, several future electron-positron colliders have been proposed for precise Higgs measurement. Such colliders could probe an inverse $0\nu\beta\beta$ decay process when converted to an electron-electron machine. In a recent study [51], it is clearly shown that the signal cross section could reach the fb level when there are three heavy Majorana neutrinos (N_I, $I = 1, 2, 3$) with hierarchical masses $M_1 \ll M_2 \ll M_3$. The mixing $|V_{e2}|^2$ of the second heavy Majorana neutrino N_2 could be large for $e^-e^- \to W^-W^-$ signal production because the $|V_{e1}|^2$ and $|V_{e3}|^2$ are suppressed by the hierarchical mass relation. In the meantime, the GERDA and KamLAND-Zen constraints could be avoided by destructive interference between N_1 and N_2. On the other hand, a detailed collider phenomenology study is missing in previous studies. The purpose of this paper is to fill in the gap by studying all decay channels and focusing on the kinematic methods to reduce background influence on sensitivity. In Sec. II, we discuss the kinematic properties of the $e^-e^- \to W^-W^-$ process and how to use it to reduce background events. In Sec. III, we show the detection possibilities in all channels with numerical analysis results. In the last section, we give a brief conclusion of this study.

II. SIGNAL AND BACKGROUND ANALYSIS

The inverse $0\nu\beta\beta$ decay could be detected in pure leptonic, semileptonic, and pure hadronic W^-W^- decay channels. In Fig. 2, according to [51], we reproduce the cross section $\sigma(e^-e^- \to W^-W^-)$ varying with M_2 in the case of three heavy Majorana neutrinos with hierarchical masses $M_1 \ll M_2 \ll M_3$. In the following, we discuss the kinematic features of each channel and the corresponding methods to separate the signal events from the large backgrounds.

A. Pure leptonic: $e^-e^- \to W^-W^- \to 2\ell + \not{E}_T$

In the pure leptonic channel, the two final-state leptons always move back to back because W^-W^- is from a spin-zero system, and only left-handed electrons take part in the weak interaction. This leads to a lepton angular-distribution peaking at $\cos\theta_{ll} = -1$. The $\cos\theta_{ll}$ cut could be applied to distinguish signals from backgrounds.

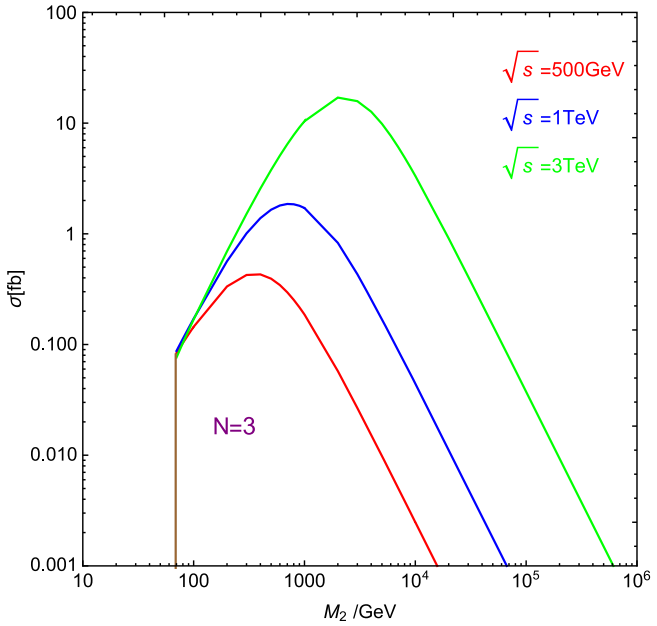

FIG. 2. The production cross sections of $e^-e^- \to W^-W^-$ with $\sqrt{s} = 500$ GeV (red line), 1 TeV (blue line), and 3 TeV (green line).

On the other hand, the two invisible neutrinos make it impossible to completely reconstruct the W bosons with $\not{E}_T$ information. The M_{T2} method could be used in this case by defining a minimization of all possible matches of $\not{p}_1$ and $\not{p}_2$ variables as [52]

$$M_{T2}^2 \equiv \min_{\not{p}_1+\not{p}_2=\not{p}_T}[\max\{m_T^2(p_T^\ell, \not{p}_1), m_T^2(p_T^\ell, \not{p}_2)\}], \quad (2)$$

where $\not{p}_T$ is the missing transverse momentum and m_T is the reconstructed transverse mass. The M_{T2} variable has an upper bound at m_W, and the corresponding $\not{p}_{1,2}$ could be used to reconstruct the system invariant mass, whose distribution is around $\sqrt{s}$ for signal events. In addition, the distinct boost effects of final-state particles should be taken into account when the collision energy is raised to several TeV, which provides us with more kinematic handles on data sample reconstructions. We thus assume that the highly boosted neutrino and lepton from the same W boson move approximately along the same direction. The relation $\vec{p}^{\,\nu} \simeq \kappa \vec{p}^{\,\ell}$ can now be applied, and κ is solved as

$$\kappa = \frac{\not{p}_T}{\sqrt{(\vec{p}_T^{\,\ell_1} + \vec{p}_T^{\,\ell_2})^2}}. \quad (3)$$

Now that the four momentums of the invisible neutrinos are obtained with this approximation, the invariant-mass cut could still be applied.

B. Semileptonic: $e^-e^- \to W^-W^- \to \ell' + 2j/j_W + \not{E}_T$

The semileptonic decay has a larger signal production rate than the pure leptonic one, and it is possible to reconstruct the W^-W^- system. For the only missing neutrino in this symmetric collision, we can easily get its momentum with $\not{E}_T$,

$$\vec{p}_\nu = -\sum_i \vec{p}_{\text{observed}}. \quad (4)$$

The two on-shell W bosons are then reconstructed either with a pair of jets or with the lepton and neutrino. Similarly, when the collision energy is raised to a few TeV, the boost effect becomes non-negligible and the two jets from W^- decay would form a fat W jet(j_W) with mass around M_W.

C. Pure hadronic: $e^-e^- \to W^-W^- \to 4j/2j_W$

In the hadronic channel with multijet final states, the W bosons could be reconstructed with proper choices of jet pairs, and the invariant mass of the four jets is required to be compared with $\sqrt{s}$. If the collision is energetic enough, the appearance of two W jets is a key feature of this hadronic decay channel.

D. Background processes

The backgrounds of the $e^-e^- \to W^-W^-$ process in different decay channels are listed in Table I. We would include those processes with extra electrons because of the abundance of background electrons at an ee collider. These extra electrons could fake $\not{E}_T$ if they are not really detected,

TABLE I. Backgrounds of the inverse $0\nu\beta\beta$ decay process and the decay channels to which they contribute.

Process	$e^-e^- + \not{E}_T$	$e^-\mu^- + \not{E}_T$	$\mu^-\mu^- + \not{E}_T$	$e^- + 2j + \not{E}_T$	$\mu^- + 2j + \not{E}_T$	$4j$
$e^-e^- \to W^-W^-\nu_e\nu_e$	•	•	•	•	•	•
$e^-e^- \to ZW^-e^-\nu_e$	•	•		•	•	•
$e^-e^- \to W^-e^-\nu_e$	•	•		•		
$e^-e^- \to Ze^-e^-$	•			•		
$e^-e^- \to ZZe^-e^-$	•			•		•
$e^-e^- \to W^+W^-e^-e^-$				•	•	•
$\gamma\gamma \to W^+W^-$				•	•	•

especially in the effective gauge-boson approximation and vector-boson fusion processes. In addition, the photon radiated from the beam electron should also be considered because the cross section of backgrounds initiated from $\gamma\gamma$ collision is comparable with other channels. Its contribution is calculated in the effective photon approximation with the improved Weizsaecker-Williams formula [53].

III. NUMERICAL RESULTS

In this section, we focus on the Monte Carlo analysis of the inverse $0\nu\beta\beta$ decay process. The simulation is performed with MadGraph5_v1.5.14 [54] and pythia-pgs [55]. In order to get more kinematic features from boost effects, we choose two benchmark points with $\sqrt{s} = 500$ GeV and $\sqrt{s} = 3$ TeV separately. According to the previous study [51], the signal of inverse $0\nu\beta\beta$ decay with only one or two Majorana neutrino flavors is too small to be detected. For this reason, we include three heavy Majorana neutrinos in the spectrum as $M_1 = 3$ GeV, $M_2 = 350$ GeV, and $M_3 = 35$ TeV when $\sqrt{s} = 500$ GeV, while $M_1 = 3$ GeV, $M_2 = 3$ TeV, and $M_3 = 300$ TeV when $\sqrt{s} = 3$ TeV. The hierarchical mass relation $M_1 \ll M_2 \ll M_3$ suppresses $|V_{e1}|^2$ and $|V_{e3}|^2$ to several orders smaller than $|V_{e2}|^2$, and we take the $|V_e|^2_{\rm EW}$ value in (1) for $|V_{e2}|^2$ accordingly. The basic cuts on final states are

$$\begin{aligned} p_T^\ell &> 10\ \text{GeV}, \qquad p_T^j > 20\ \text{GeV}, \\ |\eta^\ell| &< 2.5, \qquad |\eta^j| < 5, \\ \Delta R_{\ell\ell} &> 0.4, \qquad \Delta R_{\ell j} > 0.4. \end{aligned} \tag{5}$$

In addition, the two selected jets in the first benchmark are required to satisfy $\Delta R_{jj} > 0.4$.

In Fig. 3, we plot SM background cross sections varying with $\sqrt{s}$. The cross sections except for $e^-e^- \to ZZe^-e^-$ are always larger than 1 fb. In order to find feasible discovery channels, we start event selection with the tagging process, which requires proper final states in each channel. For example, if more than the required electrons are detected in the rapidity coverage region of the detector, they should come from background processes with extra electrons; thus, we discard this event. After that, kinematic cuts are applied to eliminate background events to obtain a better signal-to-background rate.

A. Pure leptonic

With the M_{T2} method in the first benchmark and the collinear approximation in the second, we plot the reconstructed invariant-mass $m_{\rm inv}$ distributions in the $e^-e^- + \not{E}_T$ channel, which includes most backgrounds, in Figs. 4(a) and 4(b). In order to illustrate the lepton angular correlation feature, we plot the distribution of $\cos\theta_{\ell\ell}$ in Fig. 4(c). We find that the signal $m_{\rm inv}$ distribution has an obviously distinguishable peak position from the

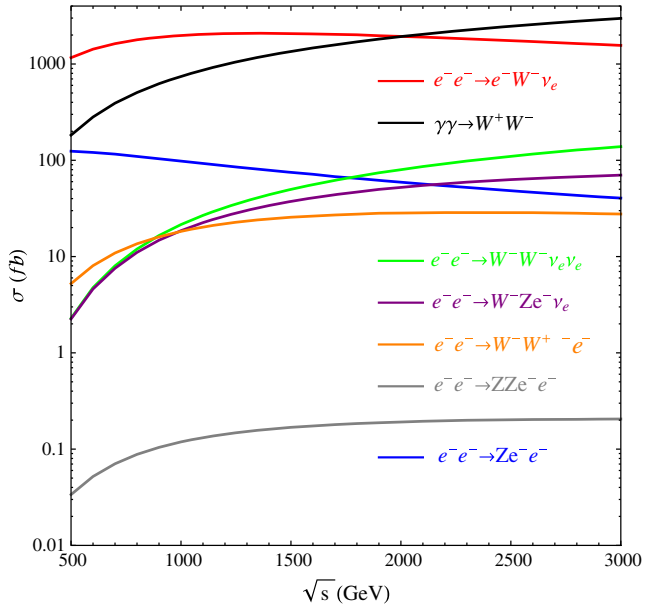

FIG. 3. SM background cross sections with different $\sqrt{s}$ values.

backgrounds except for the Ze^-e^- process. More than that, the leptons in Ze^-e^- tend to move more in the opposite directions than in other backgrounds. Although this Ze^-e^- background has similar kinematic properties to the e^-e^- signal, it should be absent in the $e^-\mu^-$ and $\mu^-\mu^-$ channels.

In Tables II and III, we list the cross sections after basic cuts, the survival probabilities after each kinematic cut, and the number of survived events N after all cuts. Note that "..." means it is not applicable in the corresponding case. We assume the invariant-mass and $\cos\theta_{ll}$ cuts are independent. The $m_{\rm inv}$ cut is different in electron and muon channels in order to deal with different background contributions. The $\cos\theta_{\ell\ell}$ cut in the second benchmark is more severe because the signal leptons are from more boosted W bosons.

B. Semileptonic channel

The semileptonic channel can be completely reconstructed because there is only one invisible neutrino in the final states. The system reconstructed with $\not{E}_T$ and leptons is identified as a W boson, whose mass distribution could be used to cut out the $W^-e^-\nu_e$ background in the $e^- + 2j + \not{E}_T$ channel. The $\gamma\gamma \to W^+W^-$ also contains a reconstructable W pair, but we use an invariant-mass cut to suppress it. In Figs. 5(a) and 5(b), the $m_{\rm inv}$ and m_W distributions in the $e^- + 2j + \not{E}_T$ channel are presented. The distributions of the $\gamma\gamma \to W^+W^-$ and $e^-e^- \to W^-e^-\nu_e$ processes can mimic the signal m_W and $m_{\rm inv}$ distributions, respectively, but not both. In the 3-TeV case, the hadronic W is identified as j_W according to the discussion in the last section.

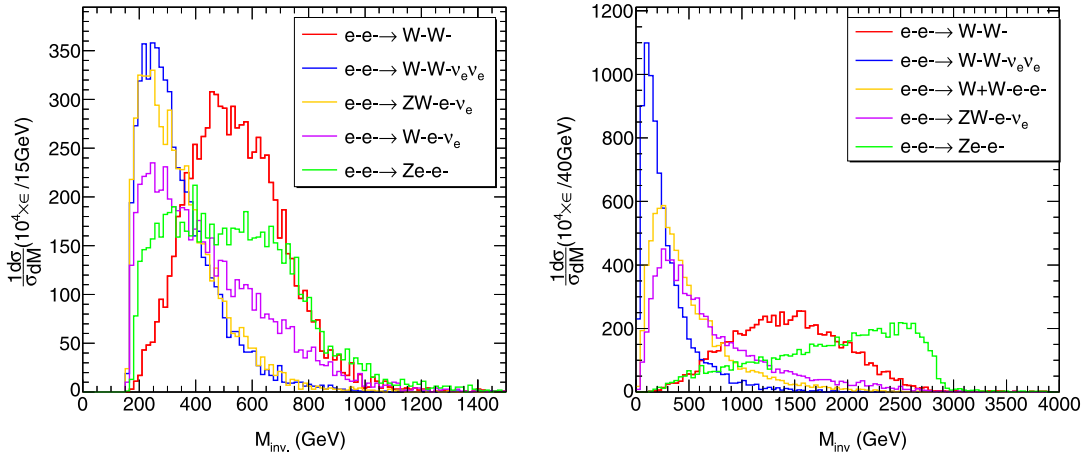

(a) $m_{\rm inv}$ distribution, $\sqrt{s} = 500$ GeV (b) $m_{\rm inv}$ distribution, $\sqrt{s} = 3$ TeV

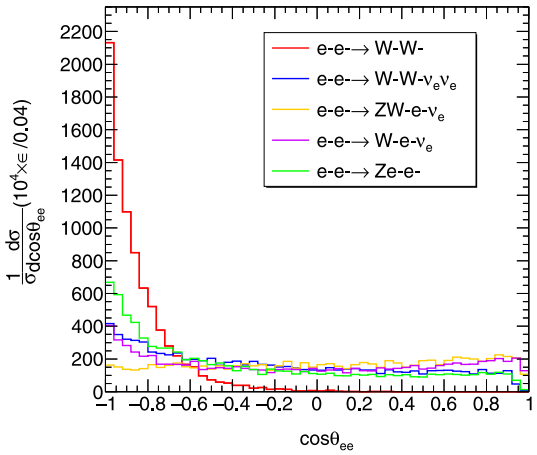

(c) $\cos\theta_{ee}$ distribution, $\sqrt{s} = 500$ GeV

FIG. 4. Kinematic features of signal and backgrounds in the pure leptonic mode. Note that ϵ is the tagging efficiency.

TABLE II. Cross section and cut efficiencies in the pure leptonic mode with $\sqrt{s} = 500$ GeV and $\mathcal{L} = 500$ fb^{-1}.

Process	$\sigma(fb)$	$\epsilon_{\rm tagging}$	$\epsilon_{m_{\rm inv}>400\ {\rm GeV}}$	$\epsilon_{\cos\theta_{ll}<-0.7}$	N
$e^-e^- + \not{E}_T$ channel					
$e^-e^- \to W^-W^-$	5.0×10^{-3}	0.84	0.68	0.591	1
$e^-e^- \to W^-W^-\nu_e\nu_e$	2.57×10^{-2}	0.83	0.15	0.042	0
$e^-e^- \to ZW^-e^-\nu_e$	4.7×10^{-2}	0.84	0.17	0.024	0
$e^-e^- \to W^-e^-\nu_e$	120.8	0.83	0.3	0.069	4168
$e^-e^- \to Ze^-e^-$	24.7	0.84	0.5	0.185	2285
$e^-\mu^- + \not{E}_T$ channel					
$e^-e^- \to W^-W^-$	1.0×10^{-2}	0.87	0.70	0.603	3
$e^-e^- \to W^-W^-\nu_e\nu_e$	5.14×10^{-2}	0.85	0.16	0.045	1
$e^-e^- \to ZW^-e^-\nu_e$	4.7×10^{-2}	0.85	0.17	0.024	0
$e^-e^- \to W^-e^-\nu_e$	120.8	0.80	0.29	0.069	4168
$\mu^-\mu^- + \not{E}_T$ channel					
$e^-e^- \to W^-W^-$	5.0×10^{-3}	0.90	0.73	0.633	1
$e^-e^- \to W^-W^-\nu_e\nu_e$	2.57×10^{-2}	0.87	0.16	0.044	0

TABLE III. Cross section and cut efficiencies in the pure leptonic mode with $\sqrt{s} = 3$ TeV and $\mathcal{L} = 500$ fb^{-1}.

Process	$\sigma(fb)$	$\epsilon_{\text{tagging}}$	$\epsilon_{0.9\text{ TeV}<m_{\text{inv}}<1.9\text{ TeV}}$	$\epsilon_{m_{\text{inv}}>900\text{ GeV}}$	$\epsilon_{m_{\text{inv}}>700\text{ GeV}}$	$\epsilon_{\cos\theta_{ll}<-0.95}$	N
$e^-e^- + \not{E}_T$ channel							
$e^-e^- \to W^-W^-$	0.18	0.82	0.52	⋯	⋯	0.52	47
$e^-e^- \to W^-W^-\nu_e\nu_e$	1.3	0.83	0.03	⋯	⋯	0.0018	1
$e^-e^- \to ZW^-e^-\nu_e$	1.15	0.83	0.1	⋯	⋯	0.0024	1
$e^-e^- \to W^-e^-\nu_e$	124.5	0.83	0.18	⋯	⋯	0.0173	1077
$e^-e^- \to Ze^-e^-$	8	0.82	0.29	⋯	⋯	0.152	608
$e^-\mu^- + \not{E}_T$ channel							
$e^-e^- \to W^-W^-$	0.37	0.86	⋯	0.72	⋯	0.72	133
$e^-e^- \to W^-W^-\nu_e\nu_e$	2.6	0.83	⋯	0.03	⋯	0.0018	2
$e^-e^- \to ZW^-e^-\nu_e$	1.15	0.82	⋯	0.11	⋯	0.0027	2
$e^-e^- \to W^-e^-\nu_e$	124.5	0.83	⋯	0.23	⋯	0.0222	1382
$\mu^-\mu^- + \not{E}_T$ channel							
$e^-e^- \to W^-W^-$	0.18	0.90	⋯	⋯	0.83	0.8208	74
$e^-e^- \to W^-W^-\nu_e\nu_e$	1.3	0.82	⋯	⋯	0.06	0.0037	2

The M_W and M_{inv} cuts are powerful in signal event selection, and we list the survival efficiencies and event numbers after successive cuts in Tables IV and V.

C. Pure hadronic

In the hadronic decay channel, the four jets are chosen to reconstruct the complete system. The invariant-mass distributions of each process are shown in Fig. 6. It is clear that m_{4j} distributions of the backgrounds deviate significantly from $\sqrt{s}$ either because there are undetected leptons carrying away part of the energy or because the process is a photon-photon scattering. In the $\sqrt{s} = 3$ TeV case, the tagging process requires two highly boosted W jets with jet mass around m_W and a small enough cone size. We further require that the separation between two W jets be larger than 0.4. The gauge bosons from the backgrounds are not that boosted since electrons and neutrinos in final states carry away large energy. This is also true for the $\gamma\gamma$ process because radiated photons are not as energetic as the electrons. We find that the cone size values, which could be estimated with the separations between W hadronic decay final states, are, in general, larger in background events. Thus, the background events can hardly meet the j_W tagging criteria. The detailed survival efficiency and number of events after implementing all cuts are list in Tables VI and VII.

D. Detection possibility

Finally, we use the signal-to-background ratio $\frac{S}{B}$ and significance $s = \frac{S}{\sqrt{S+B}}$ to evaluate the detection possibility

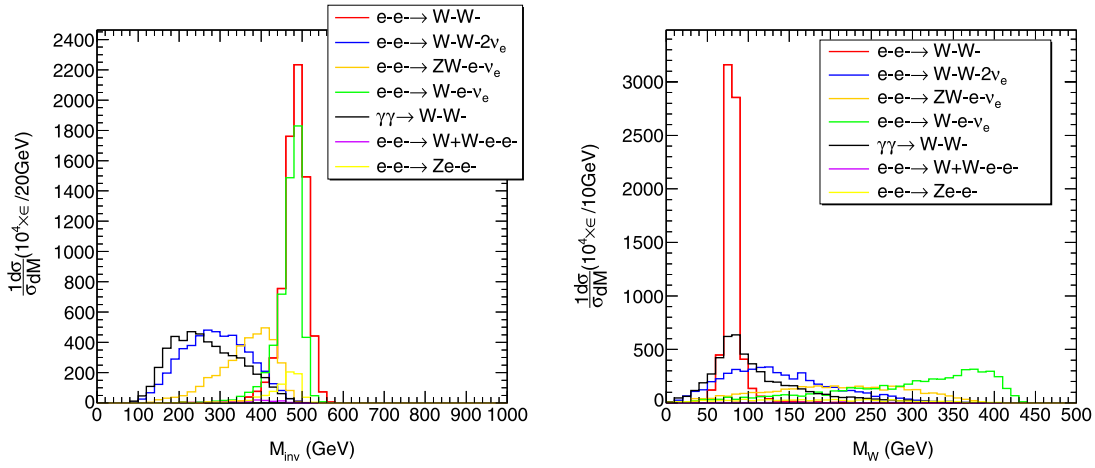

(a) m_{inv} distribution, $\sqrt{s} = 500$ GeV (b) m_W distribution, $\sqrt{s} = 500$ GeV

FIG. 5. The m_{inv} and m_W distributions of the reconstructed system in the $e^- + 2j + \not{E}_T$ channel with $\sqrt{s} = 500$ GeV. Note that ϵ is the tagging efficiency.

TABLE IV. Cross section and cut efficiencies in the semileptonic channel with $\sqrt{s} = 500$ GeV and $\mathcal{L} = 500$ fb^{-1}.

Process	$\sigma(fb)$	$\epsilon_{\text{tagging}}$	$\epsilon_{400\text{ GeV}<m_{\text{inv}}<550\text{ GeV}}$	$\epsilon_{m_{\text{inv}}>400\text{ GeV}}$	$\epsilon_{70<m_W<90\text{ GeV}}$	N
$e^- + 2j + \not{E}_T$ channel						
$e^-e^- \to W^-W^-$	5.64×10^{-2}	0.74	0.72	⋯	0.6	17
$e^-e^- \to W^-W^-\nu_e\nu_e$	0.23	0.52	0.046	⋯	0.003	0
$e^-e^- \to ZW^-e^-\nu_e$	0.3	0.37	0.13	⋯	0.002	0
$e^-e^- \to W^-e^-\nu_e$	537.3	0.54	0.51	⋯	0.007	1880
$e^-e^- \to W^+W^-e^-e^-$	0.23	0.01	0.004	⋯	0.0002	0
$e^-e^- \to Ze^-e^-$	49.1	0.08	0.07	⋯	0.003	74
$\gamma\gamma \to W^+W^-$	8 fb	0.51	0.037	⋯	0.006	24
$\mu^- + 2j + \not{E}_T$ channel						
$e^-e^- \to W^-W^-$	5.64×10^{-2}	0.74	⋯	0.72	0.6	17
$e^-e^- \to W^-W^-\nu_e\nu_e$	0.23	0.52	⋯	0.05	0.002	0
$e^-e^- \to ZW^-e^-\nu_e$	0.1	0.04	⋯	0.01	0.0004	0
$e^-e^- \to W^+W^-e^-e^-$	0.23	0.037	⋯	0.0008	0.0001	0
$\gamma\gamma \to W^+W^-$	8	0.49	⋯	0.04	0.003	12

TABLE V. Cross section and cut efficiencies in semileptonic channel with $\sqrt{s} = 3$ TeV and $\mathcal{L} = 500$ fb^{-1}.

Process	$\sigma(fb)$	$\epsilon_{\text{tagging}}$	$\epsilon_{m_{\text{inv}}>2.5\text{ TeV}}$	N
$e^- + j_W + \not{E}_T$ channel				
$e^-e^- \to W^-W^-$	2.2	0.78	0.77	847
$e^-e^- \to W^-W^-\nu_e\nu_e$	13.2	0.062	0.0032	21
$e^-e^- \to ZW^-e^-\nu_e$	9.1	0.065	0.0064	29
$e^-e^- \to W^-e^-\nu_e$	774.5	0.098	0.018	6970
$e^-e^- \to W^+W^-e^-e^-$	1.143	0.0013	0.0003	0
$e^-e^- \to Ze^-e^-$	15.76	0.008	< 0.0001	0
$\gamma\gamma \to W^+W^-$	113	0.006	0.0003	17
$\mu^- + j_W + \not{E}_T$ channel				
$e^-e^- \to W^-W^-$	2.2	0.75	0.75	825
$e^-e^- \to W^-W^-\nu_e\nu_e$	13.2	0.06	0.0026	17
$e^-e^- \to ZW^-e^-\nu_e$	2.4	0.0034	< 0.0001	0
$e^-e^- \to W^+W^-e^-e^-$	1.143	0.0009	0.0001	0
$\gamma\gamma \to W^+W^-$	113	0.005	0.0002	11

in each channel with $\mathcal{L} = 500$ fb^{-1}. The channels in which inverse $0\nu\beta\beta$ decay could be detected are listed in Table VIII. For $\sqrt{s} = 3$ TeV channels with a large signal-to-background ratio, the approximate expression for s is not valid, but we argue that the detection could be achieved through event counting. The pure hadronic

TABLE VI. Cross section and cut efficiencies in the hadronic channel with $\sqrt{s} = 500$ GeV and $\mathcal{L} = 500$ fb^{-1}.

Process	$\sigma(fb)$	$\epsilon_{\text{tagging}}$	$\epsilon_{m_{4j}>400\text{ GeV}}$	N
$4j$ channel				
$e^-e^- \to W^-W^-$	0.16	0.66	0.64	51
$e^-e^- \to W^-W^-\nu_e\nu_e$	0.5	0.35	0.0006	0
$e^-e^- \to W^+W^-e^-e^-$	1	0.004	0.0005	0
$e^-e^- \to ZW^-e^-\nu_e$	0.4	0.04	0.0008	0
$\gamma\gamma \to W^+W^-$	34.4	0.33	0.0031	53

TABLE VII. Cross section and cut efficiencies in the hadronic channel with $\sqrt{s} = 3$ TeV and $\mathcal{L} = 500$ fb^{-1}.

Process	$\sigma(fb)$	$\epsilon_{\text{tagging}}$	$\epsilon_{m_{4j}>2.3\text{ TeV}}$	N
$2j_W$ channel				
$e^-e^- \to W^-W^-$	6.7	0.73	0.73	2446
$e^-e^- \to W^-W^-\nu_e\nu_e$	34.4	0.011	0.0001	2
$e^-e^- \to W^+W^-e^-e^-$	6.3	0.0001	<0.0001	0
$e^-e^- \to ZW^-e^-\nu_e$	14.3	0.0006	<0.0001	0
$\gamma\gamma \to W^+W^-$	602	0.0033	<0.0001	30

channel with $\sqrt{s} = 500$ GeV and, for $\sqrt{s} = 3$ TeV, the semileptonic channel with an electron are also viable for inverse $0\nu\beta\beta$ decay detection with 5σ significance. The $\sqrt{s} = 500$ GeV semileptonic channel with a muon and the $\sqrt{s} = 3$ TeV pure leptonic channel with $e^-\mu^-$ still require 750 fb^{-1} and 1000 fb^{-1} integrated luminosity, respectively, for a detection.

In Fig. 6, we present a comparison between the $|V_{e2}|^2$ exclusion limit in the pure hadronic decay mode with $\mathcal{L} = 500$ fb^{-1} and the EWPO bound. We find that the $\sqrt{s} = 500$ GeV option only has a limited advantage over the current bound in the region 250 GeV $\lesssim M_2 \lesssim$ 450 GeV.

TABLE VIII. Signal-to-background ratio and significance in different decay channels with $\mathcal{L} = 500$ fb^{-1}.

	$\sqrt{s} = 500$ GeV		$\sqrt{s} = 3$ TeV	
Process	$\frac{S}{B}$	s	$\frac{S}{B}$	s
$e^-\mu^- + \not{E}_T$	⋯	⋯	0.1	3.4
$\mu^-\mu^- + \not{E}_T$	⋯	⋯	37.0	8.5
$e^- + 2j/j_W + \not{E}_T$	⋯	⋯	0.1	9.5
$\mu^- + 2j/j_W + \not{E}_T$	1.4	3.1	29.5	28.2
$4j/2j_W$	0.95	5.0	76.4	49.1

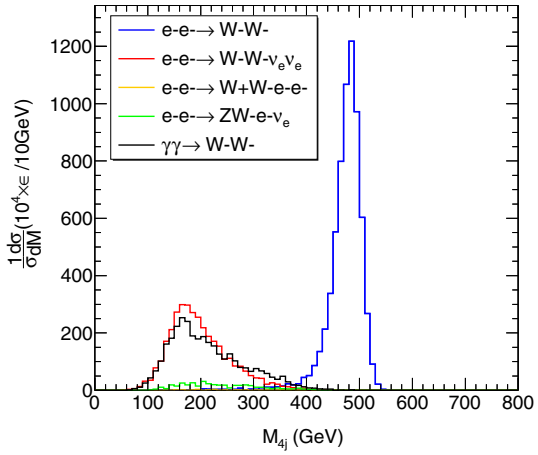

FIG. 6. m_{4j} distribution of the four-jet system, $\sqrt{s} = 500$ GeV. ϵ is the tagging efficiencies.

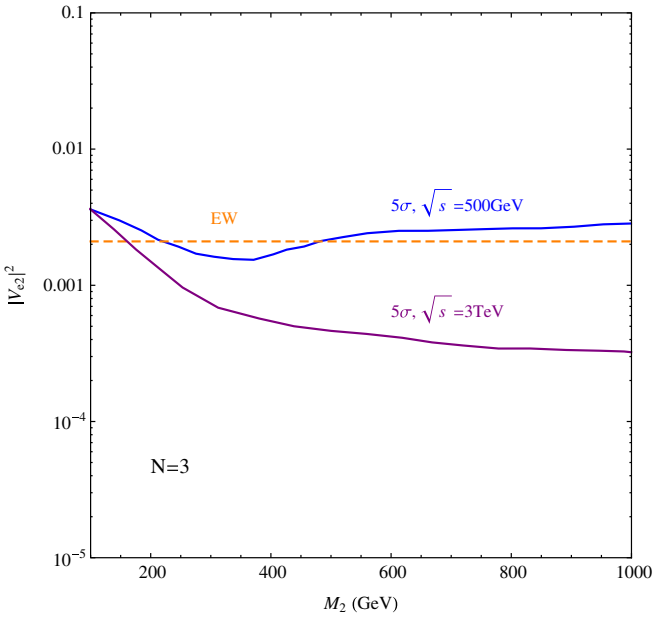

FIG. 7. The 5σ exclusion limit of $|V_{e2}|^2$ with varying M_2 in the pure hadronic channel.

But for the $\sqrt{s} = 3$ TeV case, the exclusion limit on $|V_{e2}|^2$ could reach $\mathcal{O}(10^{-4})$ when $M_2 \gtrsim 150$ GeV, providing a chance to probe Majorana neutrinos beyond EWPO experiments.

IV. CONCLUSION

The $e^-e^- \to W^-W^-$ scattering may potentially become an important realization of $0\nu\beta\beta$ decay at future electron colliders, which provides an alternative way to probe the Majorana nature of neutrinos. There are several advantages of the inverse $0\nu\beta\beta$ decay search. First of all, this process is free from the nuclear matrix element uncertainties. Second, due to the difference of energy scale from double-beta decays, the $e^-e^- \to W^-W^-$ scattering may become a complementary test to probe the LNV processes, particularly in the parameter region where significant destructive interference occurs in double-beta decays. In this study, we focus on collider phenomenology of the $e^-e^- \to W^-W^-$ process and find the kinematic features that help increase the detection potential. For example, the M_{T2} method and lepton angular distribution $\theta_{\ell\ell}$ are quite effective in the pure leptonic channel. The boost effects in the $\sqrt{s} = 3$ TeV case allow us to apply j_W tagging and the collinear approximation for W decay products. We get a better numerical analysis result in the pure hadronic channel and those channels with W decaying leptonically to a muon, while the abundant electron background's influence on $e^-e^- + \not{E}_T$ and $e^- + 2j + \not{E}_T$ channels is not a negligible issue. We then translate the results into a signal-to-background ratio and significance to evaluate the detection possibility. In the $\sqrt{s} = 500$ GeV case with $\mathcal{L} = 500$ fb^{-1}, the pure hadronic channel could already provide a 5σ detection. If we raise the collision energy to 3 TeV, the inverse $0\nu\beta\beta$ decay process could be detected in the pure hadronic channel, the semileptonic channel with a muon, and the pure leptonic channel with a dimuon simply through event counting. And if 1000 fb^{-1} data are available, 5σ detection could also be made in both the 500 GeV semileptonic channel with a muon and the 3 TeV pure leptonic channel with $e^-\mu^-$. The pure hadronic channel result is used to constrain heavy neutrino mixing in the $|V_{e2}|^2 - M_2$ plane. The result shows that the 500 GeV c.m. energy exclusion is weaker than the current EWPO bound except for a small region around 350 GeV, while the $\sqrt{s} = 3$ TeV exclusion limit is significantly stronger, reaching $\mathcal{O}(10^{-4})$. This indicates the important role of inverse $0\nu\beta\beta$ decay in future Majorana neutrino searches, especially at an electron collider with higher energy and luminosity.

ACKNOWLEDGMENTS

This work is supported in part by the National Science Foundation of China (Grants No. 11135006, No. 11275168, No. 11422544, No. 11075139, No. 11375151, and No. 11535002) and the Zhejiang University Fundamental Research Funds for the Central Universities. K. W. is also supported by the Zhejiang University K. P. Chao High Technology Development Foundation.

[1] S. M. Bilenky and S. T. Petcov, Rev. Mod. Phys. **59**, 671 (1987); **61**, 169(E) (1989); **60**, 575(E) (1988).
[2] S. M. Bilenky, C. Giunti, J. A. Grifols, and E. Masso, Phys. Rep. **379**, 69 (2003).
[3] M. C. Gonzalez-Garcia and Y. Nir, Rev. Mod. Phys. **75**, 345 (2003).
[4] C. Q. Geng and R. E. Marshak, Phys. Rev. D **39**, 693 (1989).
[5] K. S. Babu and R. N. Mohapatra, Phys. Rev. D **41**, 271 (1990).
[6] H. F. Dylla and J. G. King, Phys. Rev. A **7**, 1224 (1973).
[7] J. Baumann, J. Kalus, R. Gahler, and W. Mampe, Phys. Rev. D **37**, 3107 (1988).
[8] G. Barbiellini and G. Cocconi, Nature (London) **329**, 21 (1987).
[9] S. Weinberg, Phys. Rev. Lett. **43**, 1566 (1979).
[10] P. Minkowski, Phys. Lett. **67B**, 421 (1977).
[11] R. N. Mohapatra and G. Senjanovic, Phys. Rev. Lett. **44**, 912 (1980).
[12] T. Yanagida, Conf. Proc. **C7902131**, 95 (1979).
[13] M. Gell-Mann, P. Ramond, and R. Slansky, Conf. Proc. **C790927**, 315 (1979).
[14] M. Agostini *et al.* (GERDA Collaboration), Phys. Rev. Lett. **111**, 122503 (2013).
[15] A. Gando *et al.* (KamLAND-Zen Collaboration), Phys. Rev. Lett. **110**, 062502 (2013).
[16] L. Wolfenstein, Phys. Lett. **107B**, 77 (1981).
[17] C. N. Leung and S. T. Petcov, Phys. Lett. **145B**, 416 (1984).
[18] R. Aaij *et al.* (LHCb Collaboration), Phys. Rev. Lett. **112**, 131802 (2014).
[19] D. Liventsev *et al.* (Belle Collaboration), Phys. Rev. D **87**, 071102 (2013).
[20] F. Bergsma *et al.* (CHARM Collaboration), Phys. Lett. **166B**, 473 (1986).
[21] P. Vilain *et al.* (CHARM II Collaboration), Phys. Lett. B **343**, 453 (1995); **351**, 387(E) (1995).
[22] A. Vaitaitis *et al.* (NuTeV and E815 Collaborations), Phys. Rev. Lett. **83**, 4943 (1999).
[23] G. Bernardi *et al.*, Phys. Lett. B **203**, 332 (1988).
[24] A. V. Artamonov *et al.* (E949 Collaboration), Phys. Rev. D **91**, 052001 (2015); **91**, 059903(E) (2015).
[25] J. Badier *et al.* (NA3 Collaboration), Z. Phys. C **31**, 341 (1986).
[26] S. A. Baranov *et al.*, Phys. Lett. B **302**, 336 (1993).
[27] A. M. Cooper-Sarkar *et al.* (WA66 Collaboration), Phys. Lett. **160B**, 207 (1985).
[28] E. Gallas *et al.* (FMMF Collaboration), Phys. Rev. D **52**, 6 (1995).
[29] P. Astier *et al.* (NOMAD Collaboration), Phys. Lett. B **506**, 27 (2001).
[30] M. Aoki *et al.* (PIENU Collaboration), Phys. Rev. D **84**, 052002 (2011).
[31] R. S. Hayano *et al.*, Phys. Rev. Lett. **49**, 1305 (1982).
[32] P. Abreu *et al.* (DELPHI Collaboration), Z. Phys. C **74**, 57 (1997); **75**, 580(E) (1997).
[33] G. Aad *et al.* (ATLAS Collaboration), J. High Energy Phys. 07 (2015) 162.
[34] V. Khachatryan *et al.* (CMS Collaboration), J. High Energy Phys. 04 (2016) 169.
[35] V. Khachatryan *et al.* (CMS Collaboration), Phys. Lett. B **748**, 144 (2015).
[36] S. Antusch and O. Fischer, J. High Energy Phys. 10 (2014) 094.
[37] F. F. Deppisch, P. S. Bhupal Dev, and A. Pilaftsis, New J. Phys. **17**, 075019 (2015).
[38] M. Drewes and B. Garbrecht, arXiv:1502.00477.
[39] A. Atre, T. Han, S. Pascoli, and B. Zhang, J. High Energy Phys. 05 (2009) 030.
[40] G. Belanger, F. Boudjema, D. London, and H. Nadeau, Phys. Rev. D **53**, 6292 (1996).
[41] T. G. Rizzo, Phys. Lett. **116B**, 23 (1982).
[42] D. London, G. Belanger, and J. N. Ng, Phys. Lett. B **188**, 155 (1987).
[43] J. Gluza and M. Zralek, Phys. Rev. D **52**, 6238 (1995).
[44] W. Rodejohann, Phys. Rev. D **81**, 114001 (2010).
[45] B. Ananthanarayan and P. Minkowski, Phys. Lett. B **373**, 130 (1996).
[46] D. A. Dicus, D. D. Karatas, and P. Roy, Phys. Rev. D **44**, 2033 (1991).
[47] J. Gluza and M. Zralek, Phys. Lett. B **362**, 148 (1995).
[48] J. Gluza and M. Zralek, Phys. Lett. B **372**, 259 (1996).
[49] C. Greub and P. Minkowski, *eConf C* 960625, NEW149 (1996) Int. J. Mod. Phys. A **13**, 2363 (1998).
[50] S. Banerjee, P. S. B. Dev, A. Ibarra, T. Mandal, and M. Mitra, Phys. Rev. D **92**, 075002 (2015).
[51] T. Asaka and T. Tsuyuki, Phys. Rev. D **92**, 094012 (2015).
[52] C. G. Lester and D. J. Summers, Phys. Lett. B **463**, 99 (1999).
[53] V. M. Budnev, I. F. Ginzburg, G. V. Meledin, and V. G. Serbo, Phys. Rep. **15**, 181 (1975).
[54] J. Alwall, M. Herquet, F. Maltoni, O. Mattelaer, and T. Stelzer, J. High Energy Phys. 06 (2011) 128.
[55] T. Sjostrand, S. Mrenna, and P. Z. Skands, J. High Energy Phys. 05 (2006) 026.